Materials Advances

ROYAL SOCIETY OF CHEMISTRY

PAPER

View Article Online
View Journal | View Issue

Cite this: *Mater. Adv.*, 2021, 2, 2097

Highly broadband NLO response of acceptor–donor–acceptor materials with a planar conformation†

Yulin Huang, [ab] Wenfa Zhou, [cd] Xiaofang Li,[b] Li Jiang *[ae] and Yinglin Song *[cd]

Received 24th November 2020,
Accepted 8th February 2021

DOI: 10.1039/d0ma00918k

rsc.li/materials-advances

The third-order nonlinear optical properties of A–D–A structural molecules which are originally used as acceptors in organic photovoltaic (OPV) devices were investigated in solution and film to deeply understand the molecular conformation–property relationship. Firstly, a planar structure (O-IDTBR) bearing the indacenodithiophene (IDT) core and a twisted molecule (IDFBR) comprising the indenofluorene (IDF) core, which possess identical acceptor units, were measured by the *Z*-scan technique at the near-infrared region in toluene solution. O-IDTBR exhibits a more superior TPA cross section than IDFBR in the range of 800–1030 nm (*ca.* 1497–8811 GM). In particular, the TPA cross section of the planar configuration is 8811 GM, over 4 times that of the twisted molecule at 800 nm. Secondly, their corresponding spin-coating films are investigated *via* a 4f coherent imaging experiment at 532 nm. It is noticeable that the nonlinear refractive index of the planar molecule is up to 2.09–2.15 $\times$ 10^{-15} m^2 W^{-1}, which is nearly 5 times that of IDFBR. The dynamic processes and morphologies of films are systematically characterized by transient absorption spectroscopy and AFM. The investigations present a better understanding of the structure–property relationship of the A–D–A conjugated materials which are believed to have promising NLO application in the future.

Introduction

Nonlinear optical (NLO) materials have giant potential application in optical limiting, data storage, and optical-controllable switching.[1–3] Therefore, the materials have attracted considerable attention in recent years. Owing to their advantages of low cost, architectural flexibility and fast response speed, organic nonlinear optical materials are believed to be potentially applicable nonlinear optical materials.[4–6] Generally, the nonlinear optical properties are regulated by multiple factors, including the conjugated length, intramolecular charge transfer (ICT) and molecular conformation.[7–9] Thus, diverse strategies were performed to optimize NLO performance through synthesizing molecules with various donor and acceptor groups.[10–12] The A–D–A type molecules have emerged as outstanding electron acceptors in organic photovoltaics (OPV) with high power conversion efficiency (PCE). Additionally, due to a highly conjugated π-system, strong intramolecular charge transfer (ICT) and high electron mobility, the A–D–A type molecules are expected to show large NLO response. Recently, a series of quadrupolar A–D–A (A–π–D–π–A) chromophores exhibited large nondegenerate two-photon absorption (NDTPA) cross-sections (*ca.* 6–27 $\times$ 10^3 GM) in the near-infrared region.[13] However, the study on the NLO properties of A–D–A as mentioned above mainly focus on increasing the number of rings to modify the conjugated length and changing terminal groups to regulate the ICT. More factors, such as the influence of the molecular conformation on NLO performance, remain unknown. Moreover, the ICT properties of compounds are governed not only by the inherent features of their component moieties but also by their molecular packing.[14] Therefore, the molecular configuration should be another important factor to enhance NLO performance in theory. The fully comprehensive understanding of the structure–property relationship of A–D–A type materials is undoubtedly necessary. In this context, a planar A–D–A molecule (O-IDTBR and EH-IDTBR) and a twisted conformation

[a] *Beijing National Laboratory for Molecular Sciences, Key Laboratory of Molecular Nanostructure and Nanotechnology, Institute of Chemistry, Chinese Academy of Sciences, Beijing 100190, China. E-mail: jiangli@iccas.ac.cn*
[b] *Key Laboratory of Theoretical Organic Chemistry and Functional Molecules, Ministry of Education, School of Chemistry and Chemical Engineering, Hunan University of Science and Technology, Xiangtan, Hunan 411201, China*
[c] *Department of Physics, Harbin Institute of Technology, Harbin 150001, China. E-mail: ylsong@hit.edu.cn*
[d] *School of Optoelectronic Science and Engineering, Soochow University, Suzhou 215006, China*
[e] *University of Chinese Academy of Sciences, Beijing 100049, China*

† Electronic supplementary information (ESI) available. See DOI: 10.1039/d0ma00918k

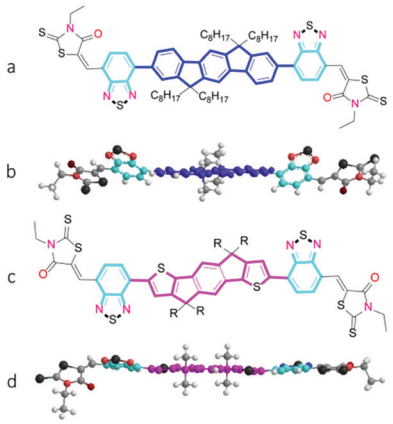

Fig. 1 Chemical structure of A–D–A molecules used in the study and corresponding optimized conformation as calculated by DFT (B3LYP/6–31G(d,p)) with methyl groups replacing alkyl chains for clarity;(a and b) IDFBR. (c and d) O-IDTBR (R = *n*-octyl) or EH-IDTBR (R = 2-ethylhexyl).

molecule (IDFBR) were chosen to perform contrast study[15,16] the chemical structures of which are displayed in Fig. 1. Because a steric clash was generated between the IDF and BT units, a more twisted conformation with a dihedral angle of 33° for IDFBR was calculated by density functional theory (DFT) methods.[17] By contrast, O-IDTBR was essentially planar because the increased quinoidal character of the phenyl–thienyl bond reduced steric twisting and enhanced the planarity compared to the phenyl–phenyl bond.[15] The O-IDTBR and IDFBR are investigated by broadband femtosecond *Z*-scan measurement in toluene. Meanwhile, the NLO response of their correspding spin coating films are fully investigated with 4f coherent imaging technique. The morphology and excited-state dynamics of the films were comprehensively studied by atomic force microscopy (AFM) and femtosecond transient absorption spectroscopy.

Results and discussion

UV-vis absorption and fluorescence spectroscopy

As shown in Fig. 2a, the maximum absorption peak of IDFBR appears at 502 nm while those of O-IDTBR and EH-IDTBR appear at 642 nm. The lower-energy peak, resulting from the highest occupied molecular orbital (HOMO) to lowest unoccupied molecular orbital (LUMO) transition, has obviously redshifted (140 nm) for O-IDTBR and EH-IDTBR, which is due to their more electron-rich core as well as more planar molecular structure.[17,18] The emission peaks of IDFBR, O-IDTBR and EH-IDTBR are located at 637 nm, 745 nm and 738 nm in CH_2Cl_2 solution when the excited wavelength is set to the maximum absorption wavelength, respectively. A pronounced positive solvatochromic effect is observed in different polarity solvents (Fig. S1, ESI†). With increasing solvent polarity, the fluorescence maximum peak in emission spectra shows a bathochromic shift accompanied by a decrease of fluorescence intensity, which clearly indicates the existence of the ICT process.[19,20] Additionally, the absorption of O-IDTBR and EH-IDTBR films exhibits a shoulder peak compared with IDFBR, which is attributed to the aggregation of indacenodithiophene-*co*-benzothiadiazole (IDT-BT).[21] The maximum emission peaks of IDFBR, O-IDTBR and EH-IDTBR appear at 622 nm, 784 nm and 766 nm in the solid film state and the maximum absorption wavelength is set to excitation wavelength.

The morphology of film images

AFM is one of the most effective methods to observe the surface morphology of spin-coating films. As shown in the AFM images in Fig. 3 and the corresponding 3D images in Fig. S2 (ESI†), the IDFBR film (Fig. 3a) takes on the amorphous surface while O-IDTBR (Fig. 3b) and EH-IDTBR (Fig. 3c) show a more well-ordered crystalline morphology. The well-ordered crystallization of O-IDTBR and EH-IDTBR should result from the planar backbone to allow effective π-stacking in the solid state, while twisted IDFBR is not conducive to stacking as well as crystallization and consequently displays an amorphous surface.[15,16] The side chain has a great impact on the intermolecular packing to make the O-IDTBR film and EH-IDTBR film arrange in different ways, where EH-IDTBR displays a closed morphology while O-IDTBR shows a loose morphology as shown in AFM images.[15,22]

Z-scan experiment

To determine the nonlinear optical properties, the femtosecond *Z*-scan experiment was conducted. The output wavelength of *Z*-scan was tuned to 800 nm, 900 nm, and 1030 nm to characterize the NLO response in toluene. As shown in Fig. 4, it is obvious that the samples show a deep valley at the zero position, which is characteristic of the reverse saturable absorption (RSA). Moreover, O-IDTBR exhibits a much deeper valley than IDFBR, indicating that O-IDTBR has stronger NLO response than IDFBR at given wavelengths. Considering the extremely

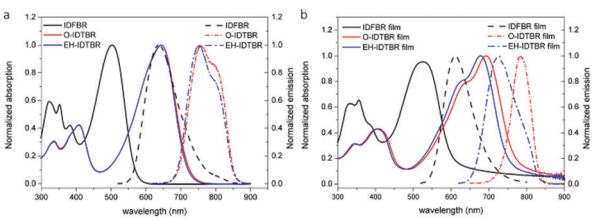

Fig. 2 Normalized UV-vis absorption (solid lines) and fluorescence spectra (dot lines) in dilute CH_2Cl_2 solution in (a) and in solid film (b).

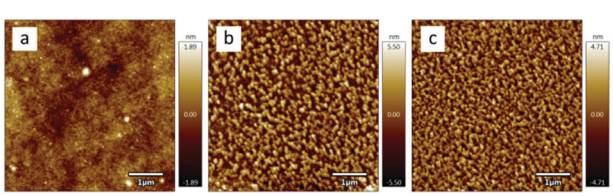

Fig. 3 AFM images of (a) IDFBR, (b) O-IDTBR and (c) EH-IDTBR on a silicon wafer in the 5 μm × 5 μm region.

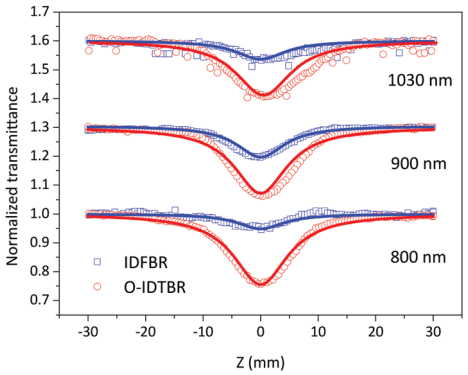

Fig. 4 Femtosecond open aperture *Z*-scan curves at 800 nm, 900 nm and 1030 nm in toluene; solid lines represent fitting curves while square and circles are experimental data.

high transmittance (up to 93%) and off-resonance excitation in the open-aperture *Z*-scan experiment, two-photon absorption (TPA) is believed to be the major mechanism of nonlinear absorption.[23] Unfortunately, the nonlinear refractive index is too weak to be observed in closed aperture *Z*-scan measurement. Through numerical simulations, the nonlinear absorption coefficient β is extracted with eqn (1),[24] $L_{\text{eff}} = \frac{1 - e^{-\alpha_0 L}}{\alpha_0}$ is the effective interaction length with the sample thickness of L, and α_0 represents the linear absorption coefficient. The third-order optical nonlinear susceptibilities χ^3 are also obtained from eqn (2),[25] the TPA cross section σ_{TPA} is calculated through eqn (3)[8] and the molecular second hyperpolarizability γ is acquired using the following eqn (4).[26] All parameters are summarized in Table 1.

$$T_{\text{Norm}}(z) = \sum_{m=0}^{\infty} \left(\frac{-\beta I_0 L_{\text{eff}}}{1 + z^2/z_0^2} \right)^m \Big/ (1+m)^{3/2} \quad (1)$$

$$\text{Im}\ \chi_{\text{eff}}{}^3 = \lambda c n_0^2 \beta / 640\pi^3 \quad (2)$$

$$\sigma_{\text{TPA}} = \hbar\omega\beta/N \quad (3)$$

$$\gamma = \frac{\chi_{\text{eff}}{}^3}{N[(n_0^2+2)/3]^4} \quad (4)$$

From the fitting results, we can find that both IDFBR and O-IDTBR possess broadband NLO response and large TPA cross sections in the near infrared (NIR) region. It is worth noting that the efficient nonlinear absorption coefficient (β_{eff}) of O-IDTBR (up to 20×10^{-13} m W^{-1}) is almost 6 times higher than that of IDFBR (3.5×10^{-13} m W^{-1}). Meanwhile, the TPA cross section of O-IDTBR is 8811 GM, which is over 4 times as much as that of IDFBR (1902 GM) at 800 nm. Because O-IDTBR exhibits better NLO properties, it can be ascribed to the combination of ICT and coplanar molecular conformation. However, as reported in the literature, the more twisted IDFBR has more localized HOMO and LUMO wavefunctions, leading to stronger charge transfer (CT)-like character than O-IDTBR.[17] Briefly, IDFBR possesses stronger ICT character than O-IDTBR while O-IDTBR exhibits outstanding NLO performance. Therefore, the better NLO properties of O-IDTBR should mainly originate from its more planar conformation. Moreover, the σ_{TPA} values of the A–D–A structure in the present study are large than those of NLO materials reported (Table 2).

Table 1 Third-order NLO parameters of open aperture *Z*-scan data at 800 nm, 900 nm and 1030 nm

Sample	Wavelength (nm)	β_{eff} ($\times 10^{-13}$ m W^{-1})	σ_{TPA} (GM)	χ^3 ($\times 10^{-15}$ esu)	γ ($\times 10^{-33}$ esu)
O-IDTBR	800	20	8811	58.1	32.10
	900	6	1713	14.3	7.90
	1030	4.7	1497	1.6	9.04
IDFBR	800	3.5	1902	12.7	6.93
	900	2.3	580	4.9	2.67
	1030	1.3	633	7.0	3.82

Table 2 The TPA cross section of the present study and previously reported molecule

Wavelength	σ_{TPA} (GM)	Sample (Ref.)
800 nm	8811	This work
	1902	
	203	27
	434–1115	28
	420	29
800–900 nm	130–300	30

4f coherent imaging system

The 4f coherent images are obtained at a wavelength of 532 nm with a laser duration of 190 fs and a repetition rate of 20 Hz. As shown in Fig. 5a–c are linear images of films, which are achieved at low laser intensity by placing neutral density filters (ND) before the sample. The transmitted intensity of central areas (PO) is similar to the outside annulus. In contrast, nonlinear images (d–f) are obtained at high excitation intensity. It is obvious that the PO region exhibits higher irradiance than the corresponding spherical surfaces, revealing that they have a positive nonlinear refractive index ($n_2 > 0$) which means the self-focusing effect.[31] Through numerical simulations, the nonlinear absorption coefficient β and nonlinear refractive index n_2 are extracted and listed in Table 3. The details of simulation were reported in a previous work.[32,33] As shown in the fitting results, O-IDTBR exhibits RSA and the self-focusing effect while both EH-IDTBR and IDFBR display SA and self-focusing. Nonlinear absorption characteristics are highly related to the wavelength, intensity and excited-state lifetime.[34]

Considering that the 532 nm wavelength is in the resonant region of IDFBR, the SA behaviour is attributed to the ground state bleaching (GSB).[35] All nonlinear absorption curves of EH-IDTBR exhibit RSA in toluene solution (Fig. S3, ESI†) while SA in the film, revealing molecular packing, can significantly modulate the signal of NLO response. Moreover, the side chain has a great impact on intermolecular packing. EH-IDTBR displays a closed morphology while O-IDTBR shows a loose morphology as shown in AFM images. Consequently, the SA

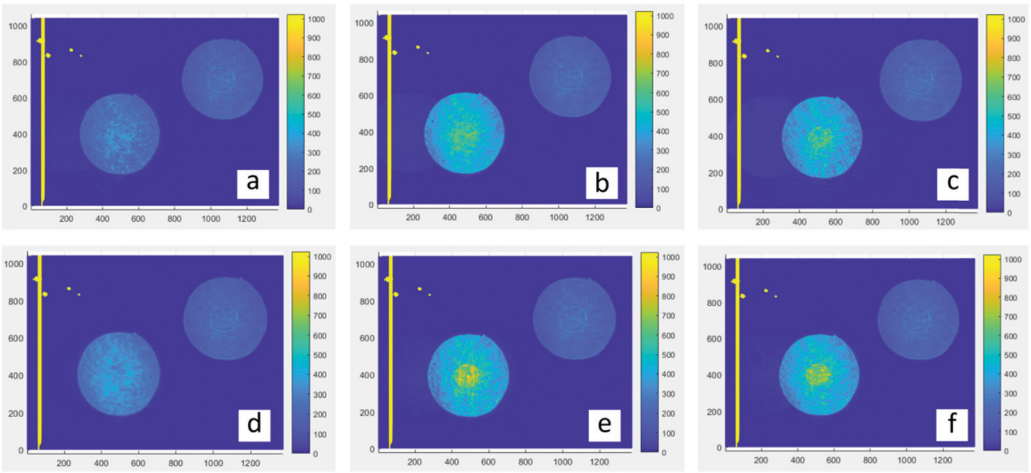

Fig. 5 Experiment images of a 4f coherent imaging system. (a–c) linear images of IDFBR, O-IDTBR and EH-IDTBR, respectively; (d–f) nonlinear imaging of IDFBR, O-IDTBR and EH-IDTBR; the central area represents the PO region.

Table 3 Third-order NLO parameters of thin films at 532 nm

Sample	β (10^{-9} m W^{-1})	n_2 (10^{-16} m^2 W^{-1})	Thickness (nm)
O-IDTBR	2.77	20.9	27
EH-IDTBR	−3.83	21.5	23
IDFBR	−4.77	4.97	38

behaviour of EH-IDTBR is mainly ascribed to different molecular packing in solid films compared to O-IDTBR.[15,36] It is remarkable that n_2 of planar molecules (O-IDTBR and EH-IDTBR) is over 4 times that of the twisted structure (IDFBR). It is believed that the planar structure enables effective π-stacking and forms a well-ordered morphology. The well-ordered arrangement would be conducive to enhance intermolecular π–π interactions, favouring more delocalization of electrons in solid states to improve the NLO properties.[37,38]

The transient absorption spectra

The TA spectra of O-IDTBR and EH-IDTBR films were recorded in the visible region under pump excitation of a 700 nm laser, while the pump wavelength is set at 500 nm for IDFBR as shown in Fig. 6. In Fig. 6b and c, positive signals from 440 to 550 nm are observed in planar molecule (O-IDTBR and EH-IDTBR) films, which are attributed to the excited-state absorption (ESA) originating from promptly photoinduced exciton (EX) or charge transfer (CT) in neat films.[39] In the first 0.45 ps, planar molecules have a weak hypsochromic shift while IDFBR (Fig. 6a) exhibits a weak blue shift in the first 0.35 ps.

According to the linear absorption of the sample film, the negative features can be assigned to ground state bleaching (GSB). Note that the maximum fluorescence emission peak of O-IDTBR and EH-IDTBR films is located at 784 nm and 766 nm, which is beyond the probe window. Meanwhile, the negative signal of IDFBR from 450 to 600 nm can be attributed to GSB, which causes the SA of IDFBR at 532 nm. The stimulated radiation (SR) of IDFBR in the 620 nm region gradually shifts to an ESA feature, which may have originated from the CT state or the pre-existing ESA dominating the SR.[8] In order to extract the decay dynamics of TA spectra, the global and target analysis with the software (carpetView) was conducted. Four dynamic processes are achieved by fitting the temporal dynamics at representative wavelengths and dynamic trace as shown in Fig. S4 (ESI†). The lifetimes of the samples are listed in Table 4. EH-IDTBR and O-IDTBR are deduced to possess a similar dynamic process because of their similar profile. The shortest lifetime corresponds to vibrational cooling in

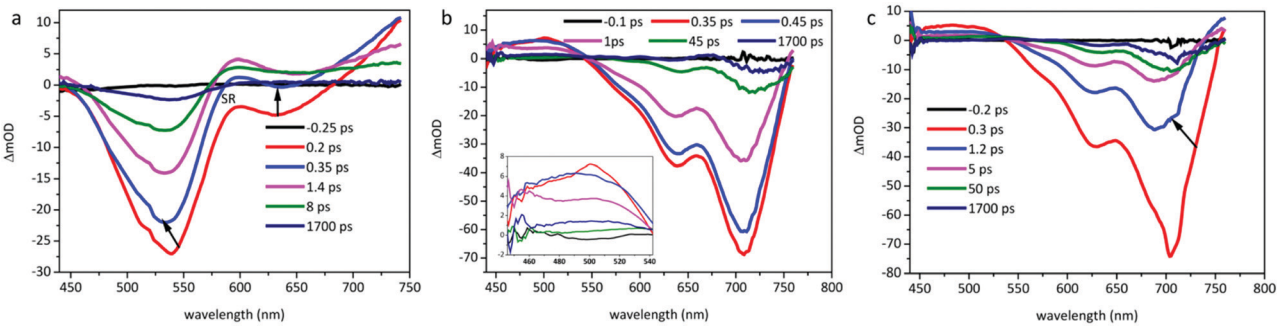

Fig. 6 Transient absorption spectra of (a) IDFBR excited at a wavelength of 500 nm, and (b) O-IDTBR and (c) EH-IDTBR excited at a wavelength of 700 nm with 190 fs laser pulses.

Table 4 Fitting lifetimes for the decay processes of thin films after laser pump excitation

	IDFBR	EH-IDTBR	O-IDTBR
LE → S_1	<250 fs	0.5 ps	0.6 ps
S_1 → S_0	3.3 ps	9.6 ps	15 ps
S_1→ CT	53 ps	85 ps	74 ps
CT → S_0	1.7 ns	1.7 ns	1.4 ns

the locally excited (LE) state. Because the time resolution of TA spectroscopy is approximately 250 fs, it is impossible to distinguish processes with a lifetime of a fewer than 250 fs. The second component with 3.3 ps lifetime is the radiative transition in the emissive state.

The third component with 53 ps lifetime represents the charge transfer process from S_1 to CT. The last component with 1.7 ns lifetime corresponds to the attenuation of CT states. Additionally, since the process of the radiative transition is much faster than that of CT states, stimulated emission is dominant and steady-state fluorescence is observed.[8] The proposed dynamic process is displayed in Fig. S5 (ESI†).

Conclusions

In summary, the influence of planar and twisted conformations on the third-order NLO properties of a series of A–D–A chromophores has been investigated in solution and in the solid state. The *Z*-scan analysis reveals that both the planar molecule and twisted molecule exhibit broadband RSA and large two-photon absorption (TPA) cross sections in solution. In particular, the TPA cross section of the planar molecule (O-IDTBR) is over 4 times that of the twisted structure (IDFBR) at 800 nm. Through numerical simulations, 4f coherent imaging measurement demonstrates that all samples display the self-focusing effect and the nonlinear refractive index n_2 of the planar molecule is nearly 5 times that of the twisted molecule. The dynamic processes and morphologies of the films are systematically characterized by transient absorption spectroscopy and AFM. Our results present a better understanding of the structure–property relationship of A–D–A chromophores and provide significant guidance for the development of excellent NLO materials in the future.

Experimental

Materials and instrumentation

All the commercial reagents were used without further purification, and the A–D–A molecules (O-IDTBR, EH-IDTBR and IDFBR) were purchased from 1-Material. The UV-VIS absorption spectrum was recorded using a HITACHI UV/VIS/NIR Spectrometer UH4150 with a concentration of 10^{-6} M and the fluorescence spectrum was collected using F-7100 of HITACHI with a concentration of 10^{-5} M at room temperature. The morphology of films was characterized by atomic force microscopy (AFM) with standard tapping mode probes (Bruker, RTESP-300) on a silica wafer.

The fabrication of solid films

Firstly, quartz substrates were cleaned with piranha solution (H_2SO_4/H_2O_2 = 3 : 1) in an ultrasonic bath for 1 h. After washing with deionized water, they were rapidly dried under high purity nitrogen. The samples are dissolved in $CHCl_3$ and the solution is filtered with a 0.22 μm filter to remove large particles before use. The samples were prepared by spin-coating from the solution directly into a pan at 3500 rpm for 30 s at room temperature, allowing the solvent to evaporate in air. The thickness of the films was determined using a profile step scanner (Bruker Dektak XT).

Z-scan measurement

In the *Z*-scan experiment, an optical parametric amplifier (OPA, ORPHEUS, Light Conversion) pumped *via* a Yb:KGW based fiber laser (PHAROS, Light Conversion) is employed as the light source. The light source can generate laser pulses with tunable wavelengths, here in *Z*-scan with a laser duration of 190 fs and a repetition rate of 20 Hz and laser pulses are tuned to 1030 nm. To minimize the influence of the thermal lens effect, a low repetition rate is used to avoid the accumulation of heat in samples. The laser pulse in the *Z*-scan experiment has a Gaussian profile. IDFBR and O-IDTBR were dissolved in toluene and the concentrations were 7.6×10^{-4} M and 7.5×10^{-4} M. The solutions were placed in 2 mm thickness quartz cells and the influence of solvent was removed from the experimental data. A schematic diagram of the *Z*-scan is shown in Fig. S6 (ESI†).

4f coherent imaging technique

The 4f coherent imaging technique with the phase object (NIT-PO) method was used to simultaneously investigate the nonlinear absorption coefficient β and nonlinear refractive index n_2 through recording the fluence distribution of laser profiles, and the schematic of the 4f coherent imaging technique is shown in Fig. S7 (ESI†). The experimental details were reported in a previous work.[31,40] The light source of the 4f system is the same as the *Z*-scan and the laser beam passes through a phase object (PO) which is placed in the input plane. The radius of the PO is 0.5 mm and the circular aperture is 1.7 mm. Since the radius of the input laser beam is larger than that of the circular aperture, a top-hat beam profile is obtained. A phase retardation of $\varphi_L = 0.5\pi$ at 532 nm is introduced into the central part of the beam when passing through the PO. After passing through the PO, the laser separates into two parts. One passes through the sample which is placed at the focal plane to investigate NLO properties, and the other is used as a reference. Lastly, the output laser beam is recorded using a CCD camera that is arranged at the output plane in the 4f system experiment. The radius of the beam is 57 μm at the focal plane with Rayleigh length (19 mm), which is thicker than the thickness of films. Among various methods of *Z*-scan techniques, the 4f coherent imaging system as a new measurement to determine third-order NLO properties has many advantages such as single laser shot, no sample movement, lower sensitivity to statistical fluctuations of the laser beam and higher sensitivity to characterize the

uneven surface of thin films.[41] Due to its advantages mentioned above, the 4f coherent imaging system is suitable to measure the third-order NLO properties of nano-films.

Femtosecond time-resolved transient absorption

To further investigate the dynamic process of the films after photoexcitation, the femtosecond transient absorption experiment was conducted. The light source is the same as the *Z*-scan. The pump wavelength is set to 500 nm and 700 nm while the spectral window of the probe is tuned in the visible region. The basic description of the transient absorption technique was available in a previous report.[42,43]

Conflicts of interest

There are no conflicts to declare.

Acknowledgements

The authors are grateful for the financial support from the National Natural Science Foundation of China (Grant No. 21673257, 51832008, and 51672280).

References

1 M. V. Vijisha, J. Ramesh, C. Arunkumar and K. Chandrasekharan, *J. Mater. Chem. C*, 2020, **8**, 12689–12697.
2 I. F. A. Mariz, F. Siopa, C. A. B. Rodrigues, C. A. M. Afonso, X. Chen, J. M. G. Martinho and E. M. S. Maçôas, *J. Mater. Chem. C*, 2015, **3**, 10775–10782.
3 L. Xu, H. Zhu, G. Long, J. Zhao, D. Li, R. Ganguly, Y. Li, Q.-H. Xu and Q. Zhang, *J. Mater. Chem. C*, 2015, **3**, 9191–9196.
4 J. Jia, X. Wu, Y. Fang, J. Yang, X. Guo, Q. Xu, Y. Han and Y. Song, *J. Phys. Chem. C*, 2018, **122**, 16234–16241.
5 Q. Feng, Y. Li, G. Shi, L. Wang, W. Zhang, K. Li, H. Hou and Y. Song, *J. Mater. Chem. C*, 2016, **4**, 8552–8558.
6 C. Xing, J. Liu, L. Yang, Z. Shao, W. Xu, Y. Zhao, K. Li, Y. Song and H. Hou, *Sci. China Mater.*, 2021, **64**, 408–419.
7 Y. Niko, H. Moritomo, H. Sugihara, Y. Suzuki, J. Kawamata and G.-I. Konishi, *J. Mater. Chem. B*, 2015, **3**, 184–190.
8 R. Niu, Y. Wang, X. Wu, S. Chen, X. Zhang and Y. Song, *J. Phys. Chem. C*, 2020, **124**, 5345–5352.
9 C. Tonnelé, B. Champagne, L. Muccioli and F. Castet, *Chem. Mater.*, 2019, **31**, 6759–6769.
10 Z. Liu, J. Sun, C. Yan, Z. Xie, G. Zhang, X. Shao, D. Zhang and S. Zhou, *J. Mater. Chem. C*, 2020, **8**, 12993–13000.
11 G. Ao, Z. Xiao, X. Qian, Z. Li, Y. Wang, X. Zhang and Y. Song, *Molecules*, 2015, **20**, 5554–5565.
12 J. Sun, B. Yuan, X. Hou, C. Yan, X. Sun, Z. Xie, X. Shao and S. Zhou, *J. Mater. Chem. C*, 2018, **6**, 8495–8501.
13 T. G. Allen, S. Benis, N. Munera, J. Zhang, S. Dai, T. Li, B. Jia, W. Wang, S. Barlow, D. J. Hagan, E. W. Van Stryland, X. Zhan, J. W. Perry and S. R. Marder, *J. Phys. Chem. A*, 2020, **124**, 4367–4378.
14 M. Kivala and F. Diederich, *Acc. Chem. Res.*, 2009, **42**, 235–248.
15 S. Holliday, R. S. Ashraf, A. Wadsworth, D. Baran, S. A. Yousaf, C. B. Nielsen, C. H. Tan, S. D. Dimitrov, Z. Shang, N. Gasparini, M. Alamoudi, F. Laquai, C. J. Brabec, A. Salleo, J. R. Durrant and I. McCulloch, *Nat. Commun.*, 2016, **7**, 11585.
16 D. Baran, R. S. Ashraf, D. A. Hanifi, M. Abdelsamie, N. Gasparini, J. A. Rohr, S. Holliday, A. Wadsworth, S. Lockett, M. Neophytou, C. J. Emmott, J. Nelson, C. J. Brabec, A. Amassian, A. Salleo, T. Kirchartz, J. R. Durrant and I. McCulloch, *Nat. Mater.*, 2017, **16**, 363–369.
17 J. Luke, E. M. Speller, A. Wadsworth, M. F. Wyatt, S. Dimitrov, H. K. H. Lee, Z. Li, W. C. Tsoi, I. McCulloch, D. Bagnis, J. R. Durrant and J. S. Kim, *Adv. Energy Mater.*, 2019, **9**, 1803755.
18 W. Zhou, Y. Fang, X. Wu, Y. Han, J. Yang, L. Shen and Y. Song, *RSC Adv.*, 2020, **10**, 19974–19981.
19 S. Zhu, K. Wang, J. Hu, R. Liu and H. Zhu, *Mater. Adv.*, 2020, **1**, 3176–3181.
20 H. Ning, Z. Yang, D. Wang, Z. Meng, Y. Li, X. Ju and C. Wang, *Microporous Mesoporous Mater.*, 2021, **311**, 110700.
21 H. Bronstein, D. S. Leem, R. Hamilton, P. Woebkenberg, S. King, W. Zhang, R. S. Ashraf, M. Heeney, T. D. Anthopoulos, J. de Mello and I. McCulloch, *Macromolecules*, 2011, **44**, 6649–6652.
22 V. K. Praveen, B. Vedhanarayanan, A. Mal, R. K. Mishra and A. Ajayaghosh, *Acc. Chem. Res.*, 2020, **53**, 496–507.
23 C. L. Devi, K. Yesudas, N. S. Makarov, V. J. Rao, K. Bhanuprakash and J. W. Perry, *J. Mater. Chem. C*, 2015, **3**, 3730–3744.
24 M. Sheik-Bahae, A. A. Said, T.-H. Wei, D. J. Hagan and E. W. Van Stryland, *IEEE J. Quantum Electron.*, 1990, **26**, 760–769.
25 Y. Cheung and S. Gayen, *J. Opt. Soc. Am. B*, 1994, **11**, 636–643.
26 S. Wang, W. Huang, T. Zhang, H. Yang, Q. Gong, Y. Okuma, M. Horikiri and Y. F. Miura, *Appl. Phys. Lett.*, 1999, **75**, 1845–1847.
27 Y. Wang, Y. Jiang, D. Liu, Y. Wang, G. Wang and J. Hua, *Appl. Phys. B: Lasers Opt.*, 2018, 124.
28 Y. Wang, G. Lai, Z. Li, Y. Ma, Y. Shen and C. Wang, *Tetrahedron*, 2015, **71**, 2761–2767.
29 D. H. Friese, A. Mikhaylov, M. Krzeszewski, Y. M. Poronik, A. Rebane, K. Ruud and D. T. Gryko, *Chemistry*, 2015, **21**, 18364–18374.
30 Ł. G. Łukasiewicz, M. Rammo, C. Stark, M. Krzeszewski, D. Jacquemin, A. Rebane and D. T. Gryko, *ChemPhotoChem*, 2020, **4**, 508–519.
31 K. Fedus and G. Boudebs, *Opt. Commun.*, 2013, **292**, 140–148.
32 Y. Li, Y. Song, Y. Wang, X. Zhang, J. Sun, J. Yang, G. Shi and Y. Wang, *Sci. China, Ser. E: Technol. Sci.*, 2008, **51**, 1483.
33 C. Li, Y. Wang, M. Shui, J. Yang, X. Jin, X. Zhang, K. Yang and Y. Song, *Opt. Commun.*, 2010, **283**, 1124–1128.

34 N. K. M. N. Srinivas, S. V. Rao and D. N. Rao, *J. Opt. Soc. Am. B*, 2003, **20**, 2470–2479.
35 S. Valligatla, K. K. Haldar, A. Para and N. R. Desai, *Opt. Laser Technol.*, 2016, **84**, 87–93.
36 D. Li, B. Li, S. Wang, C. Zhang, H. Cao, X. Tian and Y. Tian, *Spectrochim. Acta, Part A*, 2020, 224.
37 Q.-Y. Ouyang, Y.-J. Chen and C.-Y. Li, *Mater. Chem. Phys.*, 2012, **134**, 80–86.
38 J. Qin, C. An, J. Zhang, K. Ma, Y. Yang, T. Zhang, S. Li, K. Xian, Y. Cui, Y. Tang, W. Ma, H. Yao, S. Zhang, B. Xu, C. He and J. Hou, *Sci. China Mater.*, 2020, **63**, 1142–1150.
39 H. Feng, N. Qiu, X. Wang, Y. Wang, B. Kan, X. Wan, M. Zhang, A. Xia, C. Li, F. Liu, H. Zhang and Y. Chen, *Chem. Mater.*, 2017, **29**, 7908–7917.
40 Z. Li, C. He, J. Fan, Y. Wu, Y. Liu, J. Feng and Y. Song, *Mater. Lett.*, 2018, **221**, 279–281.
41 J. Sun, G. Wang, C. Liu, Y. Shi and M. Zhao, *Opt. Laser Technol.*, 2019, **109**, 600–607.
42 C. Wang, R. Niu, Z. Zhou, W. Wu, Z. Chai, Y. Song and D. Kong, *Nanotechnology*, 2020, 31.
43 Y. Chai, X. Liu, B. Wu, L. Liu, Z. Wang, Y. Weng and C. Wang, *J. Am. Chem. Soc.*, 2020, **142**, 4411–4418.